Supplementary Information for: Sources of carbonaceous aerosol in a South-East European metropolis

Stephen M. Platt[1], Milos Davidović[2], Alena Bartonova[1], Željko Ćirović[2], Sabine Eckhardt[1], Nikolaos Evangeliou[1], Hans Gundersen[1], Maja Jovanović[2], Milena Jovašević-Stojanović[2], Griša Močnik[3], Bojana Petrović[2], Philipp Schneider[1], Karl Espen Yttri[1]

[1]NILU, 2027, Kjeller, Norway
[2]VIDIS Center, Vinča Institute of Nuclear Sciences, National Institute of the Republic of Serbia, University of Belgrade, Belgrade, Serbia
[3]Center for Atmospheric Research, University of Nova Gorica, 5270 Ajdovščina, Slovenia

Correspondence to: Stephen M. Platt (sp@nilu.no), Miloš Davidović (davidovic@vin.bg.ac.rs)

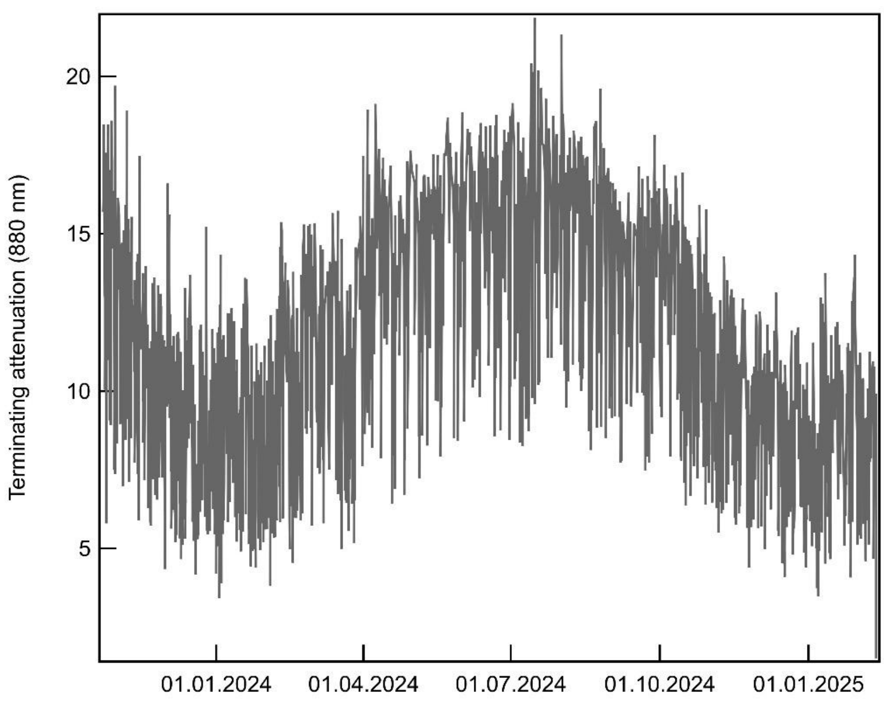

Figure S1: Time series of the terminating attenuation at 880 nm for each filter spot, defined as the final hourly attenuation value immediately preceding tape advance. Tape advance is triggered by the 370 nm channel, such that the maximum attenuation reached at 880 nm varies. The pronounced seasonal cycle reflects changes in aerosol optical properties, in particular seasonal variability in the absorption Ångström exponent (AAE), and illustrates that the end-of-spot loading state at 880 nm is not constant throughout the year with respect to attenuation at 880 nm.

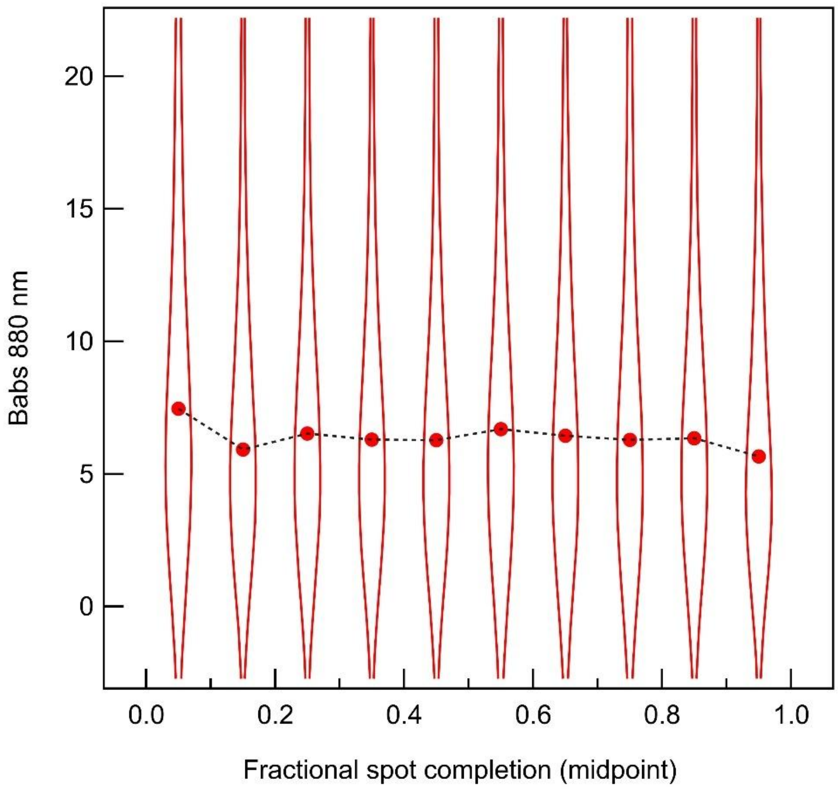

Figure S2: Distribution of the absorption coefficient at 880 nm (B_{Abs} 880 nm as a function of fractional filter spot completion, where spot progression is defined using attenuation at 880 nm. Violin plots show the distribution of hourly B_{Abs} 880 values within bins of fractional spot completion, with red markers indicating bin medians and the dashed line connecting medians across bins. The absence of a systematic trend in median B_{Abs} 880 with increasing spot completion indicates that the dual-spot loading correction effectively removes filter loading artefacts at 880 nm when spot progression is evaluated consistently at the same wavelength.

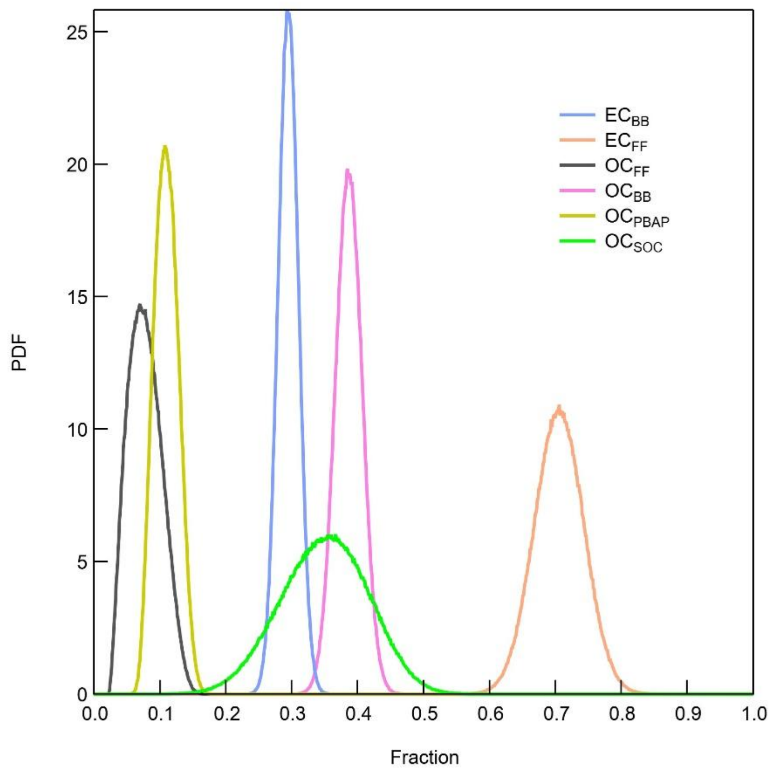

Figure S3: Probability density functions (PDFs) of fractional contributions to total elemental carbon (EC_{TOT}) and total organic carbon (OC_{TOT}) from various sources, estimated using a tracer-based Monte Carlo approach. The biomass burning fractions EC_{BB} (light blue) and OC_{BB} (pink) are shown alongside fossil fuel contributions EC_{FF} (orange) and OC_{FF} (black). Additional organic carbon sources include OC_{PBAP} (yellow), representing contributions from primary biological aerosol particles (PBAP), and OC_{SOC} (green), representing secondary organic carbon (SOC). Fractions are relative to EC_{TOT} for EC_{BB} and EC_{FF}, and to OC_{TOT} for OC_{BB}, OC_{FF}, OC_{PBAP}, and OC_{SOC}. Distributions reflect 1,000,000 Monte Carlo realisations incorporating uncertainty in input data and literature-derived source ratios.

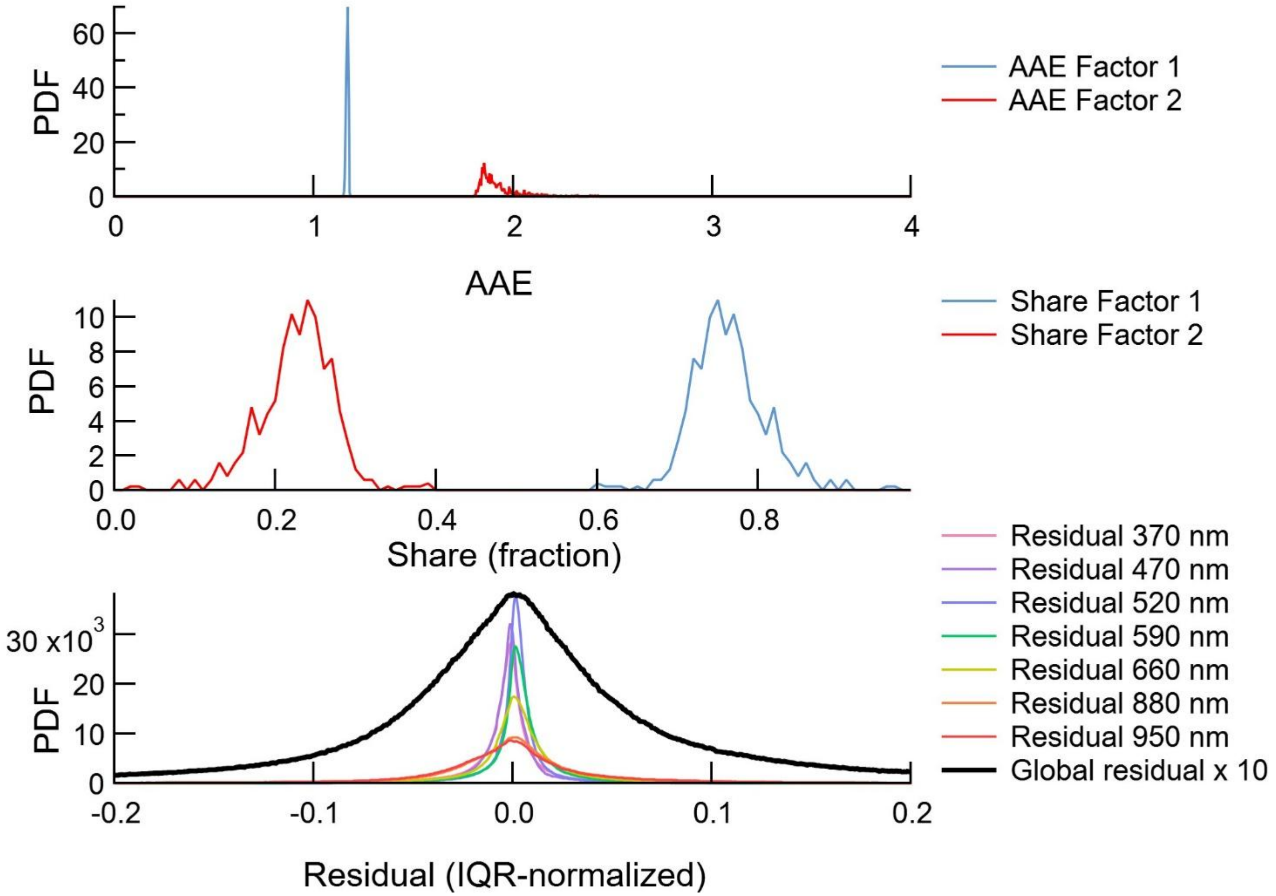

Figure S4: NNMF ensemble (500 repeat runs) diagnostics for a two-factor solution sorted by Ångström exponent (AAE). (Top) AAE distributions show two narrow, well-separated modes: a low-AAE component (mode=1.17, consistent with soot/BC from traffic and a higher-AAE component (mode=1.86, consistent with BrC-like absorption from residential wood combustion, RWC). The tight peaks indicate stable components across ensemble layers (little rotation or swapping), though factor 2 exhibits higher AAE variability than factor 1. (Middle) Share distributions (Eq. 8, main text) are also well separated, with factor 1 contributing most of the absorption (peak near ~0.75 to 0.8) and factor 2 near ~0.2 to 0.3. Limited overlap implies the factors are identifiable and not degenerate. (Bottom) Residual PDFs at each wavelength are centered at zero and narrow, and the global residual (black, ×10 for visibility) is likewise symmetric and small. The absence of systematic bias at any wavelength and the thin, nearly Gaussian cores indicate that two components capture the structure of the data without leaving patterned misfit or requiring an additional factor.

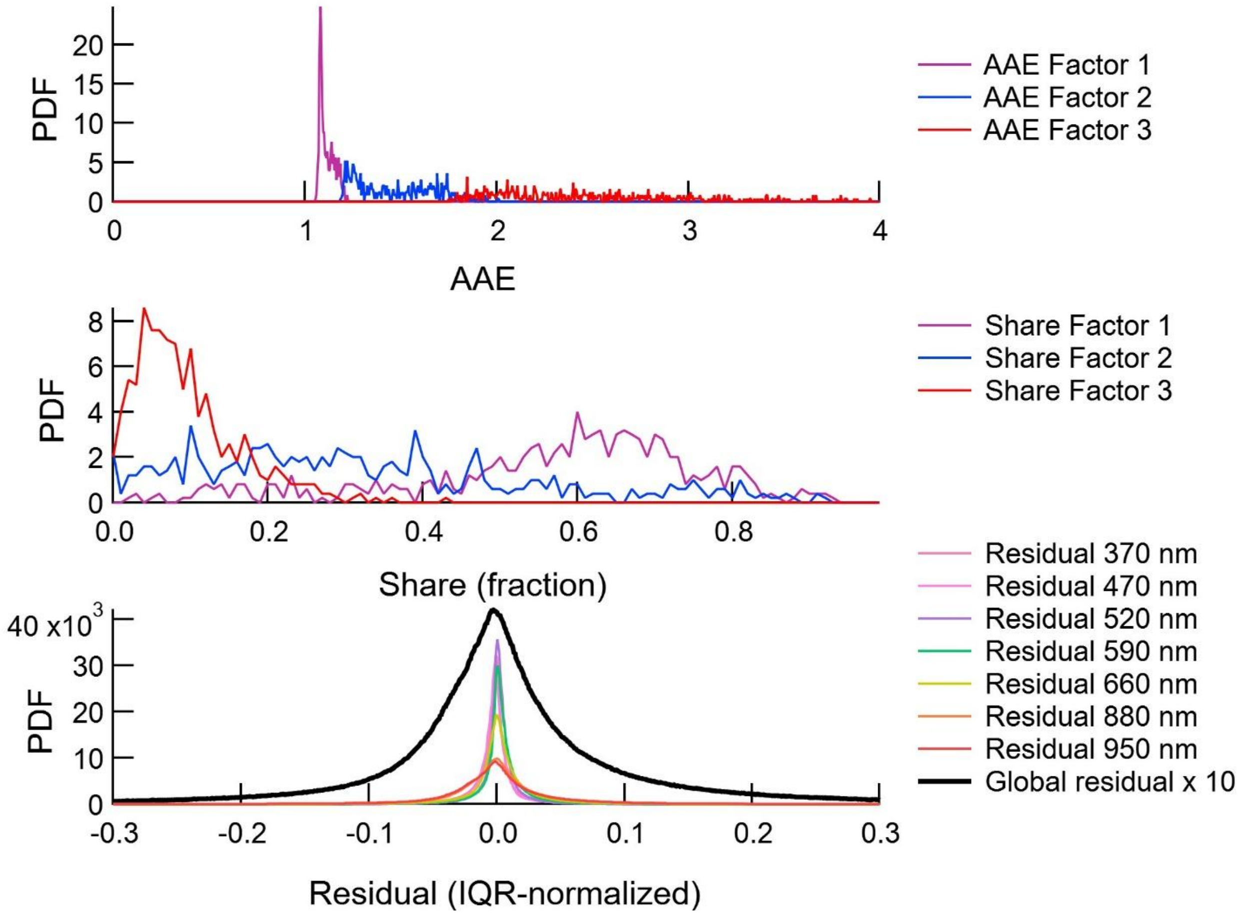

Figure S5: NNMF ensemble (500 repeat runs) diagnostics for a three-factor solution sorted by Ångström exponent (AAE). Top: AAE distributions. Factor 1 (purple) forms a sharp peak just above AAE≈1 (BC-like), but Factors 2 (blue) and 3 (red) are broad and strongly overlapping; Factor 3 shows a long tail to high AAE. The breadth/overlap indicate unstable, rotating components rather than three distinct factors. Middle: Share distributions according to Eq. 8, main text. One factor (red) is pushed to the edge with most mass near zero share, while the other two overlap substantially. Edge shares and overlap are typical signs of a redundant component. Bottom: Residual PDFs. Per-wavelength residuals remain narrow and centered at zero; the global residual (black, ×10 for visibility) is symmetric and only marginally different from the two-factor case. The extra factor does not deliver a meaningful reduction in misfit or remove systematic structure, especially since more degrees of freedom will automatically yield a smaller residual. The combination of (i) non-separated/unstable AAEs, (ii) an edge-share factor, and (iii) little to no residual improvement argues against a three-factor description of these data. A two-factor model is better supported. Introducing a third factor here likely splits noise or partitions the existing factor 2 component without adding physical meaning.

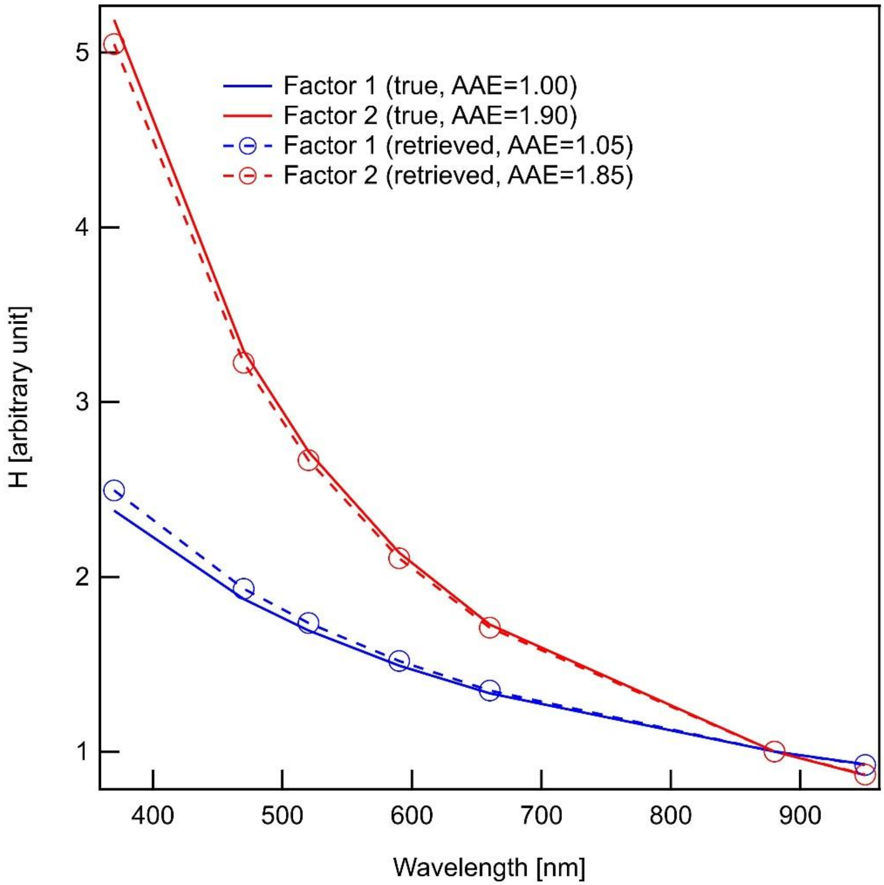

65 **Figure S6: Imposed (solid lines) and NNMF-retrieved (dashed lines with markers) factor spectra for a synthetic dataset constructed from two power-law absorption components (AAE = 1.00 and 1.90), combined with realistic temporal variability and added Gaussian noise. The NNMF ensemble median solution successfully recovers both spectral shapes, yielding AAEs of 1.05 and 1.85.**

70